Quasielastic K^+ scattering

C. M. Kormanyos,[1,*] R. J. Peterson,[1] J. R. Shepard,[1] J. E. Wise,[1] S. Bart,[2] R. E. Chrien,[2] L. Lee,[3] B. L. Clausen,[4] J. Piekarewicz,[5] M. B. Barakat,[6,†] E. V. Hungerford,[6] R. A. Michael,[7] K. H. Hicks,[7] and T. Kishimoto[8]

[1]*Department of Physics, University of Colorado, Boulder, Colorado 80309*

[2]*Brookhaven National Laboratory, Upton, New York 11973*

[3]*TRIUMF, 4004 Wesbrook Mall, Vancouver, British Columbia, V6T 2A3, Canada*

[4]*Loma Linda University, Loma Linda, California 92350*

[5]*Supercomputer Computations Research Institute, Tallahassee, Florida 32306*

[6]*Department of Physics, University of Houston, Houston, Texas 77204*

[7]*Department of Physics, Ohio University, Athens, Ohio 45701*

[8]*Department of Physics, Osaka University, Osaka, 560, Japan*

(Received 29 June 1994)

K^+-nucleus double-differential cross sections in the quasielastic region have been measured using a kaon beam with an incident laboratory momentum of 705 MeV/c. Data are presented for D, C, Ca, and Pb at fixed three-momentum transfers of 290, 390, and 480 MeV/c. Measurements of the effective number of nucleons are compared with calculations predicted from a semiclassical attenuation model based on the eikonal approximation, and the long nuclear mean free path expected for positive kaons is found, even for lead. An exclusive $(K, K'p)$ spectrum for C at 480 MeV/c is shown. The characteristics of the exclusive data suggest that protons with zero orbital angular momentum have been detected in coincidence. The inclusive data are described well by local density random phase approximation calculations which include isoscalar N-N correlations in the σ-ω model.

PACS number(s): 25.80.Nv, 21.60.Jz

I. INTRODUCTION

At sufficiently high momentum transfers the nuclear response in the quasielastic region is centered near a nuclear excitation energy equal to the kinetic energy expected to be transferred to a single ejected nucleon, broadened by the momentum distribution of the bound nucleons with a width associated with the internal momentum of the bound nucleons. At low-momentum transfers the effects of N-N correlations are important, and the distribution of quasielastic strength is influenced by nuclear collectivity. We have obtained nuclear quasielastic scattering data covering a range of three-momentum transfers extending from the regimes of single-nucleon scattering to collective scattering with a beam of K^+ mesons as a new test for models of nuclear dynamics.

There have been many studies of (e, e') quasielastic scattering [1,2], and interpretations of these have been aided by the well-understood nature and the weakness of the fundamental interaction. Similar studies with hadronic probes [3–7] in principle yield responses not accessible in (e, e') scattering. However, strong projectile-nucleon interactions can greatly complicate theoretical analyses of these studies and also prevent deep nuclear penetration by the hadronic probes used in these studies. Since there is no first order $q\bar{q}$ annihilation channel for the the K^+-N system, the fundamental K^+-N interaction is weaker than other hadron-nucleon interactions for laboratory momenta below about 800 MeV/c. Consequently the K^+ has a comparatively long nuclear mean free path in this momentum range, allowing it to penetrate more deeply into heavy, dense nuclei than other available hadronic beam particles. For example, at the incident momentum used in this experiment, which was 705 MeV/c, the classically computed mean free path of positive kaons in nuclear matter is about 4 fm, compared to about 2 fm for either pions or protons with that momentum. Thus a K^+ interacts with a larger number of nucleons at a greater density in the nucleus than does a pion or a proton.

Inclusive doubly differential (K, K') cross sections were measured for C at fixed three-momentum transfers of 290, 390, and 480 MeV/c, and for Ca and Pb at 290 and 480 MeV/c. In addition, exclusive triply differential $(K, K'p)$ cross sections were measured for C, Ca, and Pb at 480 MeV/c over a portion of the solid angle subtended by the cone of knocked-out protons.

II. EXPERIMENTAL METHOD

The experiment was performed on the C-6 beam line of the Alternating Gradient Synchrotron using the hypernuclear spectrometer system (Moby-Dick) [5]. Moby-Dick consists of a front and a rear spectrometer; both are magnetic spectrometers made up of one dipole (D)

*Present address: NIKHEF-K, 1009 DB Amsterdam, The Netherlands.

†Present address: Yale University, Department of Physics, New Haven, CT 065211.

magnet and four quadrupole (Q) magnets in a QQDQQ arrangement. The rear spectrometer has a solid angle of approximately 18 msr with an angular acceptance of 3.8°, a momentum acceptance of about 14%, an energy resolution of 3 MeV, and a flight path in the rear spectrometer of 6.6 m for the central ray. Three electronic signals for incident beam (B) pions (π), kaons (K), and protons (p) and three signals for scattered (S) particles were combined to form three trigger types πB, KB, and pB for beam particle events and three trigger types $\pi\pi$, KK, and pp for scattered ($B \times S$) particle events. The average computer live-time over the course of the experiment was 98.3% ± 0.7%.

An incident beam momentum of 705 MeV/c at the center of the targets with a momentum spread of 3.8% was used. Beam tuning gave nearly equal intensities of π^+ and K^+ on target, with a typical flux of around 2×10^5 per 0.6 s beam spill each 3.8 s and an incident proton flux of about 2×10^4 per spill. The spatial distribution of the incident K^+ beam on the scattering target had a full horizontal width of 8 cm and a full vertical height of 3 cm. Particle identification was carried out with four plastic scintillators, two before the scattering target and two after the target, used for time-of-flight measurements. In addition, a Čerenkov counter was used to identify beam pions. Trajectories of each incident particle and each scattered particle were determined with position measurements from 8 drift chambers upstream of the scattering target and 9 drift chambers downstream of the target.

A second arm composed of a single phosphor sandwich (or phoswich) was used to detect knocked-out protons and deuterons. It was composed of a scintillating plastic disk with areal density 0.41 g/cm^2 epoxied on top of a 54 g/cm^2 disk of $Bi_4Ge_3O_{12}$ (BGO). The BGO detector was thick enough to stop all the knocked-out protons and deuterons which generated a signal in the detector since the knocked-out particles had kinetic energies ranging from about 30 to 230 MeV. Furthermore, since the heavier, slower deuterons lost proportionally more of their kinetic energy in the scintillator strip, it was possible to distinguish clearly between protons and deuterons using a short 30 nsec electronic gate and a longer 270 nsec gate on the BGO detector output signal. The BGO detector was placed such that the sum of the angles between a kaon scattered at 43° and the ray through the center of the BGO detector was 94°, chosen such that an unbound stationary proton at the center of the scattering target would hit the center of the BGO detector. The area of the BGO detector was 81 cm^2, and it was placed 28 cm from the target along the ray between the center of the target and the center of the BGO detector; the solid angle of the BGO detector was roughly 110 msr. Consequently, since the solid angle subtended by the knocked-out protons from the nuclear targets exceeded the solid angle of the BGO detector, the second arm preferentially detected bound protons with zero orbital angular momentum, as suggested by previous analyses of $(K, K'p)$ kinematics in Refs. [9,10].

The momentum acceptance of the rear spectrometer was determined with 13 measurements of elastic scattering of beam protons (with the beam line retuned for protons) from hydrogen in a CH_2 target of thickness 1.16 g/cm^2, and was checked for consistency with seven data points from elastic K^+-p scattering from the hydrogen in a nylon-6 target of thickness 1.16 g/cm^2. Measurements of elastic K^+-p scattering using the nylon target, double checked using a CH_2 target of thickness 0.94 g/cm^2 and checked in yet another run the following year using a different CH_2 target of thickness 2.35 g/cm^2, were normalized to the SP88 phase shift solution [11] to obtain the cross section scale for the final spectra. The total normalization uncertainty was determined to be ±11%.

The exclusive coincidence measurements required additional normalization factors to account for protons which stopped in the scattering target or scattered outside of the BGO detector solid angle due to energy losses and/or because of nuclear reactions within the scattering target. These effects were treated simultaneously utilizing a Monte Carlo method and the total proton-nucleus cross sections of Ref. [12]. The effects of multiple small angle scattering were assumed not to contribute to the overall coincidence efficiency on average since the angular distribution of the knocked-out protons is slowly varying over the BGO detector solid angle and because the angular distribution is symmetrically centered near the center of the front face of the BGO detector.

Natural isotopic targets of CH_2, $NH(CH_2)_5CO$ (nylon-6), C, Ca, and Pb and an isotopically separated CD_2 target were used. The Ca target was wrapped in a negligibly thin layer of aluminum foil to prevent oxidation. The CH_2 and nylon targets were used for normalization and momentum acceptance measurements. Spectra were obtained for D, C, Ca, and Pb, where the contribution from the C was subtracted from the CD_2 measurements to obtain the D spectra. All the spectra were taken at fixed laboratory scattering angles of 24°, 34°, and 43°, corresponding to fixed three-momentum transfers q of 290, 390, and 480 MeV/c, respectively, computed for elastic K^+ scattering from free nucleons. However, due to the 3.8° angular acceptance of the rear spectrometer in the scattering plane as well as the fact that a fixed scattering angle does not exactly correspond (kinematically) to a fixed momentum transfer, q was only approximately constant to within about ±20 MeV/c across the full range of the broad spectra measured.

From three to five spectrometer momentum settings were required to cover the wide range of nuclear excitation energy ω in the spectra. Here the nuclear excitation energy is defined by

$$\omega \equiv \left[(\epsilon_i - \epsilon_f + m_A)^2 - (\vec{k}_i - \vec{k}_f)^2\right]^{1/2} - m_A \,, \qquad (1)$$

where ϵ_i (ϵ_f) is the initial (final) total K^+ energy in the laboratory frame, $\vec{k}_i$ ($\vec{k}_f$) is the initial (final) K^+ three-momentum in the laboratory frame, and m_A is the rest mass of the target nucleus. With this definition of ω, the peak for K^+-nucleus elastic scattering is expected to lie at an excitation energy of zero. Contributions from adjacent histograms were averaged according to their statistical weights to obtain the final spectra. The momentum of the scattered particles ranged from 350 to 700 MeV/c,

resulting in scattered K^+ survival fractions from about 8% to 28%. The nuclear targets ranged in thickness from 1 to 5 g/cm^2, introducing an energy spread in the incident and scattered particles. This energy spread combined with the spectrometer resolution gave an overall energy resolution of about 7 MeV.

Sample spectra for C at scattering angles of 43° and 24° are shown as typical examples in Fig. 1. The 43° spectrum is dominated by the broad peak centered near a nuclear excitation energy of $q^2/2M$ (where M is the nucleon rest mass) expected for quasielastic scattering, similar to observations from electron scattering. All the peaks were fit with a split Gaussian line shape to extract the FWHM peak widths, centroids, and areas. The contributions from elastic scattering and low energy excited levels were fit with a symmetric Gaussian line shape where such states were visible. A split Gaussian line shape provided a reasonable description of the quasielastic peak over the range of scattering angles and targets in this experiment. The values of χ^2 ranged from 0.5 to 2.5, with a value near 1.5 most common for the fitted inclusive spectra. Typical fits to spectra are shown in Fig. 1. For each laboratory scattering angle and each target, the singly differential cross sections were obtained from the integrated areas under the fitted quasielastic peaks without backgrounds. The uncertainty in the cross section due to fitting has been computed by varying the line shape parameters within their variance. This gave an uncertainty of about 5% in most cases, which was added in quadrature to the normalization uncertainty to obtain the total uncertainty for the final inclusive singly differential cross sections. Some of these data and a few salient conclusions have been presented [13], and a complete presentation is available from Ref. [14].

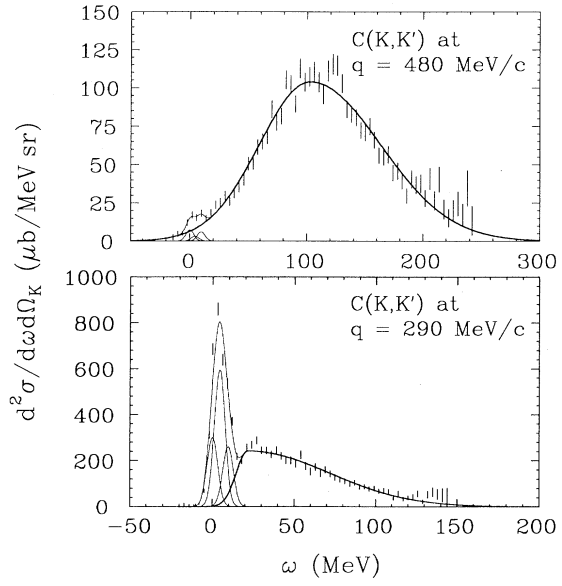

FIG. 1. The fitted data for C at 24° and 43° are shown. The quasielastic peaks have been fitted with a split Gaussian, as shown, and the elastic and low-lying excited levels have been fitted with a symmetric Gaussian line shape with a width equal to the experimentally determined energy resolution.

III. EXPERIMENTAL RESULTS

A. Inclusive cross sections

The doubly differential cross sections for positive kaons scattered from natural carbon targets are plotted in Fig. 2 versus nuclear excitation energy ω for momentum transfers of 290, 390, and 480 MeV/c (fixed scattering angles of 24°, 34°, and 43°, respectively). At 480 MeV/c the data clearly display the characteristic shape of a quasielastic peak, while at q = 290 MeV/c the quasielastic strength is concentrated at nuclear excitation energies lower than the peak location expected for free scattering, due to coherent nuclear effects. At a momentum transfer of 390 MeV/c, the characteristics of the nuclear response are between the collective and the incoherent regimes. Elastic scattering and discrete nuclear excitations are an obvious feature in the spectrum at 290 MeV/c. However, since the differential cross sections for these states tend to be highly diffractive while the angular distribution of the quasielastic peak follows the relatively flat angular

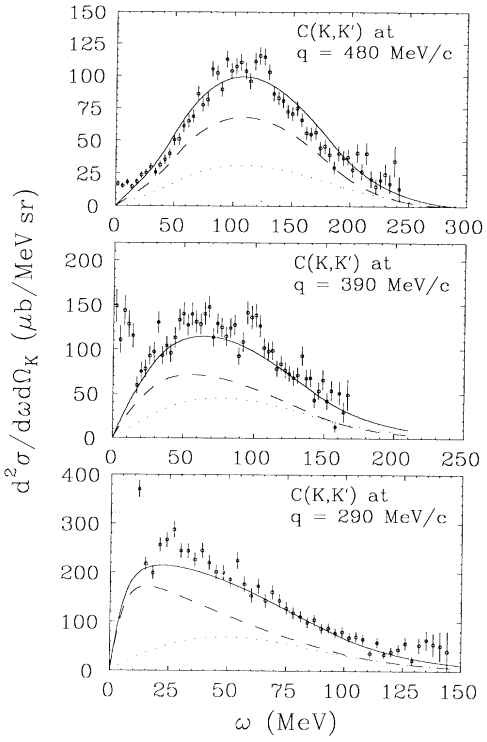

FIG. 2. K^+-C doubly differential cross sections $d^2\sigma/d\omega d\Omega_K$ are plotted as a function of nuclear excitation energy ω for scattering of positive kaons with an incident momentum of 705 MeV/c. The data were taken at fixed laboratory scattering angles of 24°, 34°, and 43°, corresponding closely to fixed momentum transfers over the full quasielastic region of 290, 390, and 480 MeV/c, respectively. The solid curve in each panel shows the sum of the isoscalar (ΔT = 0, dashed) and isovector (ΔT = 1, dotted) contributions to the local density RPA theoretical calculations described in Sec. IV. The magnitude of the predictions has been set by the measured effective number of nucleons.

distribution of the fundamental K^+-N cross section [11], the strength of the discrete levels drastically decreases in relation to the strength of the quasielastic peak with increasing momentum transfer.

The doubly differential cross sections for positive kaons scattered from natural calcium and lead are plotted in Figs. 3 and 4. Data were obtained at momentum transfers of 290 and 480 MeV/c for each of these two targets. The characteristics of the spectra for Ca and Pb at the two-momentum transfers are very similar to the features of the C spectra at the corresponding momentum transfers. However, the strength of the quasielastic peaks increases since, as will be discussed in Sec. III B, the inclusive singly-differential cross sections for hadron-nucleus quasielastic scattering tend to increase with A.

For comparison with the heavy nuclear targets, the doubly differential cross sections for D are shown in Fig. 5. Since the maximum internal nuclear momentum in D is comparatively small, the quasielastic peaks for D are not as broad as the peaks for the heavy nuclei. In addition, the trend of increasing collectivity with decreasing q which was observed for the heavy nuclei is not strongly seen in the D spectra.

B. Effective number of nucleons

In practice, quasielastic scattering of hadrons is not proportional to the full number of nucleons (A) in the nucleus but, instead, from some effective number of nucleons due to the strong distortions and interactions undergone by the scattering probe within the nucleus. The experimental values of the effective number of nucleons

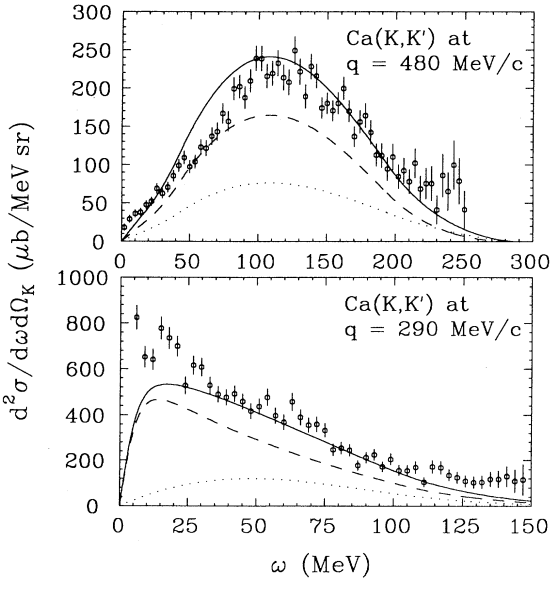

FIG. 3. Doubly differential cross sections for Ca are plotted for momentum transfers of 290 and 480 MeV/c. Local density RPA calculations are shown, as in Fig. 2. The magnitude of the predictions has been set by the measured effective number of nucleons.

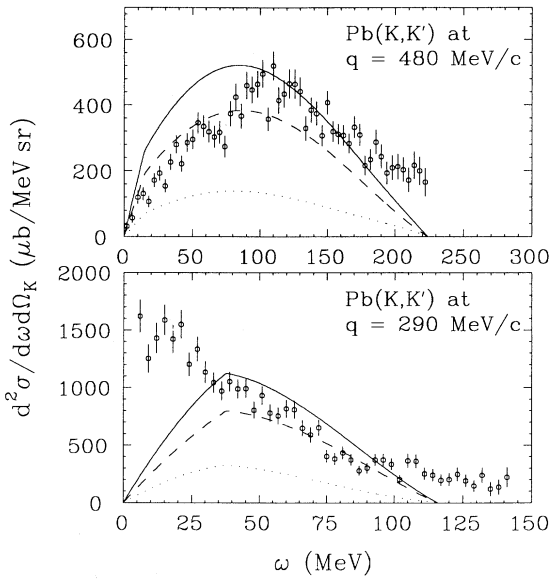

FIG. 4. Doubly differential cross sections for Pb are plotted for momentum transfers of 290 and 480 MeV/c. Uncorrelated nuclear matter (Fermi gas) calculations are shown, as in Fig. 2. The magnitude of the predictions has been set by the measured effective number of nucleons.

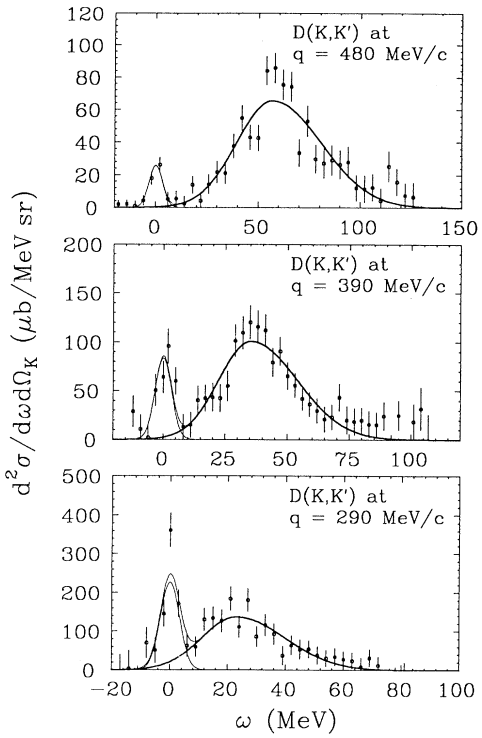

FIG. 5. Doubly differential cross sections for D are displayed for momentum transfers of 290, 390, and 480 MeV/c. The fitted spectra are shown.

have been extracted from the data at 290 and 480 MeV/c by integrating the areas under the fitted doubly differential cross sections over the quasielastic region. The corresponding effective number of nucleons $A_{\rm eff}^{\rm exp}$ is then obtained by dividing this singly differential cross section by the appropriate combination of K^+-p and K^+-n differential cross sections. These cross sections were taken to be 2.92 and 1.64 mb/sr, respectively, at 24° and 1.96 and 1.19 mb/sr, respectively, at 43° [11], in the laboratory frame.

The results for $A_{\rm eff}^{\rm exp}$ are displayed in Fig. 6. Similar to the findings of Refs. [3,4], the A dependence follows a power law

$$A_{\rm eff}^{\rm exp} = N_0 A^{\alpha} , \tag{2}$$

where N_0 and α are constants; values of $(1.8 \pm 0.4)A^{(0.61\pm0.05)}$ and $(2.0 \pm 0.4)A^{(0.61\pm0.05)}$ have been found for the data at 290 and 480 MeV/c, respectively. The exponent of 0.61 ± 0.05 found for positive kaons can be compared to the results of 0.44 ± 0.05 found for positive pion noncharge exchange (NCX) [3], 0.56 ± 0.03 for negative pion NCX [3], 0.38 ± 0.03 for pion single charge exchange (SCX) [4], and near unity for electrons.

We also calculate the effective number of nucleons considering single collisions between a K^+ and a nucleon in the nuclear volume for every incident impact parameter b in the eikonal approximation [13,15,16]:

$$A_{\rm eff}^{\rm cal} = \int d^2b T(b) e^{-\sigma_T T(b)} , \tag{3}$$

where

$$T(b) = \int_{-\infty}^{\infty} dz \rho\left(\sqrt{b^2+z^2}\right) , \tag{4}$$

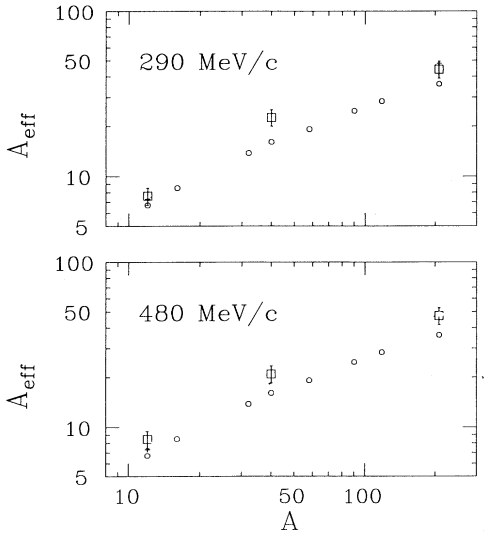

FIG. 6. The effective number of nucleons for quasielastic K^+ scattering from C, Ca, and Pb are shown for momentum transfers of 290 and 480 MeV/c. The experimental results of $A_{\rm eff}^{\rm exp}$ (squares) are compared to the calculated results of $A_{\rm eff}^{\rm cal}$ (circles).

in which $\rho(r)$ is the proton density taken from the ground state charge distributions of Ref. [17], and where the neutron density is assumed to have the same shape as the proton density. Also σ_T is the appropriately isospin averaged K^+-N total cross section determined from the K^+-p and K^+-n total cross sections of 12.40 and 15.76 mb, respectively [11]. A weakness of the use of the eikonal model for this determination of $A_{\rm eff}^{\rm cal}$ is that Eq. (3) is derived at 0°, while the values of $A_{\rm eff}^{\rm exp}$ have been determined at nonzero scattering angles. The eikonal approximation was used since it is has been found to work empirically [3,4,16,18] for hadron scattering at similar scattering angles. These calculated values are compared to those obtained from the data in Fig. 6.

The computed $A_{\rm eff}$ are below the measured values at both angles for the three heavy targets. Since enhancements of the in-medium K^+-nucleon cross sections have been put forth [19–25], it is worth examining the consequences of such an effect on our data.

Since the elementary K^+-nucleon cross sections are nearly isotropic at our beam energy, the total and differential cross sections can be taken to be proportional. A larger total cross section will decrease $A_{\rm eff}$, with each differential cross section being larger. These effects strongly tend to compensate one another.

In Fig. 7 we show the 42° differential K^+ quasielastic cross sections, divided by the number of target nucleons. The solid curve shows the eikonal prediction for these differential cross sections. When both the total and the differential cross sections per nucleon are changed by ±20% the dashed and dotted curves result. As expected, there is a strong cancellation, such that our results are strikingly insensitive to the fundamental K^+-nucleon in-medium cross sections.

With or without notice of possible unconventional medium effects or uncertainties in the fundamental cross sections, the large values of $A_{\rm eff}^{\rm exp}$ found for C, Ca, and Pb

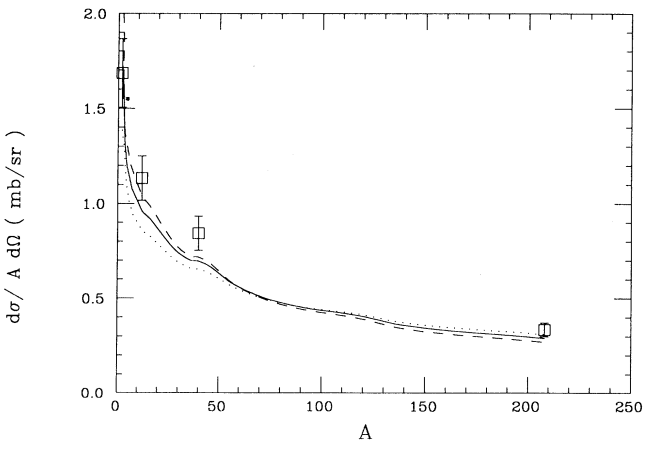

FIG. 7. Differential cross sections for K^+ quasielastic scattering (per target nucleon) are shown for 42°. Free differential cross sections, averaged for protons and neutrons, are multiplied by $A_{\rm eff}^{\rm cal}$ to yield the solid curve. Changes of both total and differential cross sections by +20% (dashes) and −20% (dots) yield almost the same curve.

confirm the nuclear penetration anticipated for the K^+. For example, we find that the effective number of protons in Pb is 18 out of 82, while for positive pion scattering at the same q the effective number of protons was found to be 13 out of 82 [3] and, similarly, only 9 out of 83 for pion SCX on Bi [4]. In addition we have calculated the radius R and fraction of the central density $\rho(R)/\rho(0)$ for which

$$A_{\rm eff}^{\rm exp} = \int_R^\infty d^3r\rho(r) \ . \tag{5}$$

Using this simple model, we find that K^+'s reach a nuclear density in Pb which is 55% of the central density, while for pion SCX, only 25% of the central density is reached.

C. Extracted Fermi momenta

For a Fermi gas of nucleons and for momentum transfers above the region of Pauli blocking, the quasielastic peak is expected to have a width (FWHM) [3]:

$$\Gamma_{\rm FG} = \frac{1}{\sqrt{2}}\left(\sqrt{(q+k_F)^2+M^2} - \sqrt{(q-k_F)^2+M^2}\right) , \tag{6}$$

where M is the nucleon rest mass and k_F is the Fermi momentum. Equation (6) has the nonrelativistic limit

$$\Gamma_{\rm NR} = \sqrt{2}\,\frac{qk_F}{M} \ , \tag{7}$$

from which we see that the quasielastic peak (for sufficiently high-momentum transfers) is expected to have a width proportional to k_F.

Values of k_F have been extracted with Eq. (6) from the widths of the fitted K^+ quasielastic peaks at the largest momentum transfer of 480 MeV/c. The results are shown in Fig. 8. There is a sharp rise in k_F from D to C with less of a change from Ca to Pb, as the densities of the heavier nuclei become saturated. Values of k_F = 73, 190, 220, and 230 MeV/c were found for D, C, Ca, and Pb, respectively.

Values of k_F have also been obtained through Eq. (6) from widths of quasielastic peaks measured in 500 MeV pion single charge exchange at 488.1 MeV/c [26–28]. The comparison of k_F values is independent of the slightly different momentum transfers. The pion data give smaller Fermi momenta, reflecting the shorter mean free path for this probe, sensing lower nuclear densities than did the K^+.

D. Coincidence measurements

Exclusive $(K, K'p)$ triply-differential cross sections were measured for D, C, Ca, and Pb at a momentum transfer of 480 MeV/c. The exclusive measurements were made in order to look for differences between the shapes

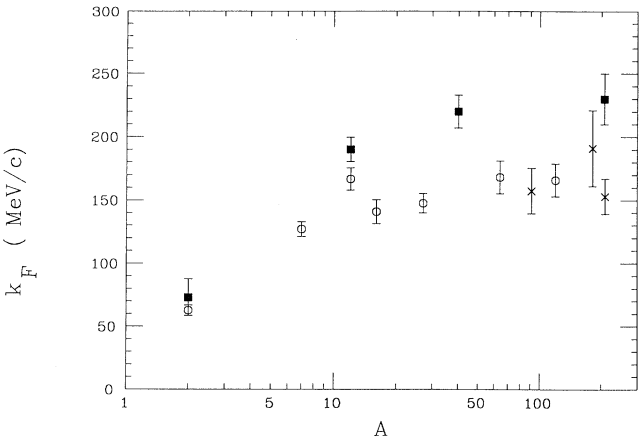

FIG. 8. Fermi momenta extracted from measured widths of quasielastic peaks are compared. Solid squares are from the present K^+ work, circles are from the average of data for (π^+, π^0) and (π^-, π^0), and crosses are for only (π^+, π^0) data [27]. The π^0 data are for an angular acceptance similar to that of the present K^+ work, and the momentum transfers are near 480 MeV/c for all data sets.

of the quasielastic inclusive and exclusive spectra. Since the BGO detector was placed near the angle for free K^+-p scattering, such differences might be attributed to very poorly resolved shell structure effects and binding energy effects, or simply due to the fact that the protons in any shell tend to be knocked out near the free recoil proton angle when they are instantaneously slower (which is on average more often for s-shell protons than for protons with nonzero orbital angular momentum).

Figure 9 shows the calibrated time-of-flight, full energy (EBGO) and partial energy loss in the plastic (dE-BGO) spectra for K^+ scattered at 43° with a hydrocarbon target and a carbon target. Scattering from hydrogen dominates the top plots, while the lower plots are from the sum of all scattered K^+ momentum settings. A clear peak is observed for carbon, and all proton energies above 25 MeV were used to form our exclusive spectrum.

The exclusive $(K, K'p)$ spectrum for C at 43° is compared to the corresponding inclusive (K, K') spectrum in Fig. 10. The coincidence spectrum peaks at an excitation energy of 130 MeV, compared to 100 MeV for the inclusive peak and the FWHM of the coincidence peak is 80 MeV, compared to 120 MeV for the inclusive peak. The coincidence spectra for all the nuclear targets feature a similar smaller width and peak shift to higher nuclear excitation energy, as well as depletion of the cross section for ω less than about 50 MeV, while the shape of the high-ω side of the peak is similar.

Previous analyses [9,10] of the angular distribution of knocked-out protons in $(K, K'p)$ reactions at similar energies have shown that the angular distribution of $L = 0$ protons is peaked at the free proton scattering angle, while the angular distribution of $L \neq 0$ protons is bimodal, with peaks on both sides of the free proton knockout angle. Many previous angular correlation studies of quasifree knockout have encountered and explained this

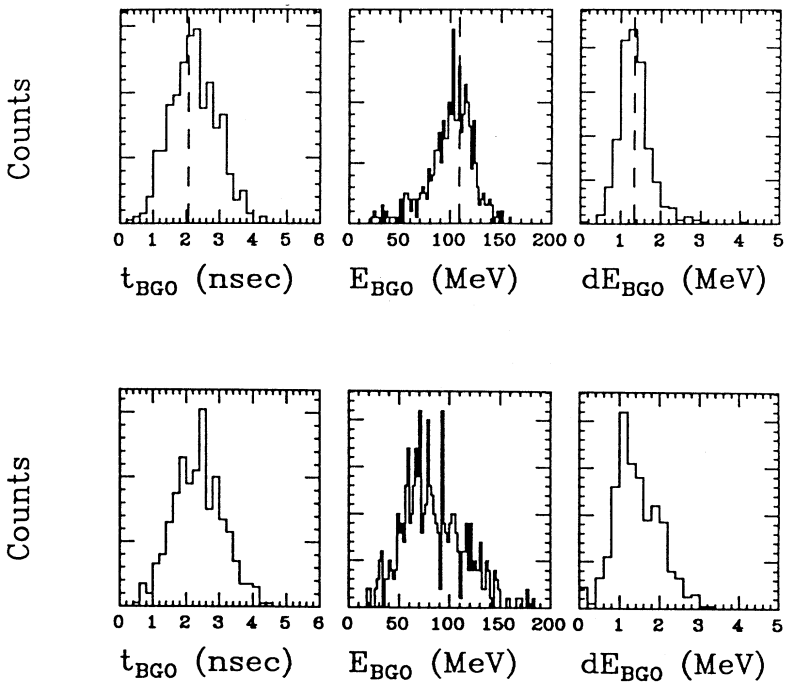

FIG. 9. Calibrated TOF, total energy deposited, and energy deposited in the thin scintillator for the BGO detector are shown in the left, center, and right panels, respectively, for a scattered K^+ angle of 43°. The results for a hydrocarbon target and for the sum of all carbon runs are shown, respectively, in the upper and lower sets of panels. The vertical dashed lines in the upper panels show the expected values of the associated measured quantity.

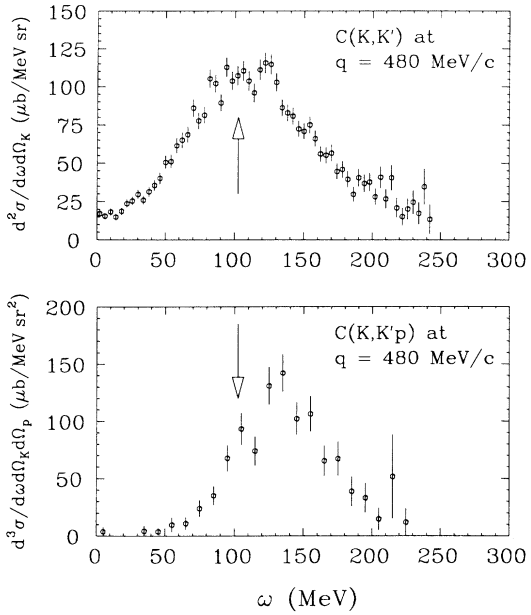

FIG. 10. The exclusive $(K, K'p)$ spectrum (lower panel) for C at 43° is compared to the inclusive (K, K') spectrum (upper panel) for C at 43°. In the $(K, K'p)$ spectrum the exclusive quasielastic peak has a smaller width and its centroid is shifted toward higher nuclear excitation energy. The arrows indicate the excitation energy which would be expected for the kinematic conditions of free K^+-p scattering.

general feature [29]. This suggests that the s-shell protons in C were preferentially detected in our coincidence, and this also agrees with the shift to higher ω which we have observed in our exclusive spectra.

IV. THEORETICAL METHODS

A. K^+-A cross section in the PWIA

Quasielastic scattering of hadrons at these momentum transfers can be described using the plane wave impulse approximation (PWIA). This gives rise to the common use of a factorized doubly differential cross section which is given schematically by [15,16]

$$\frac{d^2\sigma}{d\omega d\Omega} = \left.\frac{d\sigma}{d\Omega}\right|_{\text{free}} A_{\text{eff}}\, S(\omega, q)\ , \tag{8}$$

where $d\sigma/d\Omega|_{\text{free}}$ is the fundamental hadron-nucleon singly differential cross section at the same scattering kinematics, A_{eff} represents the effective number of nucleons participating in the scattering reaction due to distortions, and $S(\omega, q)$ is the nuclear response to the scattering probe. Aside from the couplings between the external probe and the nucleon, the nuclear response to quasielastic scattering is essentially independent of the external

probe and depends only on the properties of the nucleus; distortions in this model only influence the magnitudes of the cross sections.

For the case of K^+-nucleus scattering in the PWIA, the K^+-nucleus doubly differential cross section can be written as [13,14,16]

$$\frac{d^2\sigma}{d\omega d\Omega_K} = A_{\rm eff}^{\rm exp}\kappa\left\{|f_s|^2 S^{SS} + |f_v|^2\left[\left(\frac{\epsilon_i+\epsilon_f}{2m}\right)^2 \times\left(\frac{Q^4}{q^4}S^{00}+\frac{Q^2}{q^2}S^{11}\right)-\left(1+\frac{Q^2}{4m^2}\right)S^{11}\right] + 2{\rm Re}(f_s f_v^*)\frac{\epsilon_i+\epsilon_f}{2m}\frac{Q^2}{q^2}S^{S0}\right\}, \quad (9)$$

where $Q^2 \equiv q^2-\omega^2$, ϵ_i (ϵ_f) is the initial (final) K^+ total energy in the laboratory frame, and m is the K^+ rest mass. The relativistic invariants f_s and f_v are related to the on-shell, isospin-averaged K^+-N scattering amplitude in the K^+-N system center-of-momentum (c.m.) frame as shown in Refs. [13,14]. For all situations herein, Q^2 is greater than zero. The kinematical factor κ, arising from the transformation of the solid angle from the c.m. frame to the laboratory frame, is given by

$$\kappa = \frac{k_f}{k_i}\left(\frac{\epsilon+E}{E}\right)^2, \quad (10)$$

where ϵ is the K^+ total energy and E is the nucleon total energy in the c.m. frame. In addition, all calculations which will be shown have been scaled by the experimentally determined effective number of nucleons $A_{\rm eff}^{\rm exp}$.

The nuclear responses are given by

$$S^{ab} = -\frac{1}{\pi}{\rm Tr}\left[\theta^a\frac{\Pi(\omega,q)}{\rho}\theta^b\right] \equiv -\frac{1}{\pi}{\rm Im}\Pi^{ab}(\omega,q)/\rho\,, \quad (11)$$

where the Π^{ab} are the nuclear polarization insertions in the nuclear channels which can be excited by positive kaons (specifically the isoscalar and isovector spin-flip and non-spin-flip channels), and ρ is the nuclear density. For $a \to s$, $\theta^a \to \mathbb{1}$, while for $a \to 0$, $\theta^a \to \gamma_0$, and for $a \to 1$, $\theta^a \to \gamma\cdot\hat{e}_T$, where $\hat{e}_T$ is a unit vector in the scattering plane and perpendicular to $\vec{q}$.

While the responses S^{00} and S^{11} arise in electromagnetic (e,e') nuclear scattering, the responses S^{SS} and S^{S0} are unique to a hadronic interaction of the K^+-N form. This was anticipated since there is no scalar component in the usual representation of the fundamental electron-nucleon amplitude. The non-spin-flip charge longitudinal (or Coulomb) response S^{00} as well as the spin-flip transverse response S^{11} are related to the longitudinal and transverse (e,e') responses [2] via $S_L = S^{00}$ and $S_T = 2S^{11}$. In principle, the spin-flip process could include both the longitudinal (magnetic quantum number $M_s = 0$) as well as the transverse ($M_s = \pm 1$) responses. However, angular momentum and parity conservation forbid the spin-flip longitudinal process for K^+-N scattering. For electron scattering a Rosenbluth separation of S^{00} and S^{11} is possible by varying the incident electron energy and electron scattering angle. A similar separation for K^+ scattering could, in principle, also reveal the individual responses S^{SS} and S^{S0}. Unfortunately, such a separation is not possible for these kaon data. Thus, while the scalar-scalar and mixed scalar-vector responses are excited by the K^+, the individual responses cannot be individually extracted from the cross section data.

B. Local density random phase approximation

In order to mimic the dynamical behavior of nucleons bound within finite nuclei as well as the finite nuclear mean free path of kaons, we have performed random phase approximation (RPA) calculations using a local density approximation (LDA). In our LDA the nucleus is treated as nuclear matter of appropriate density at a given radius by computing a local Fermi momentum $k_F(r)$ and a local effective nucleon mass $M^*(r)$ at every nuclear radius. The nuclear response function at a radius r is given by

$$S^{ab}(\omega,q;r) = -\frac{1}{\pi}{\rm Im}\Pi^{ab}(\omega,q;r)/\rho(r)\,, \quad (12)$$

where $\rho(r)$ is normalized to satisfy $\int\rho(r)d^3r = A$, and the Π^{ab} are computed for nuclear matter using the local values of the Fermi momentum and effective nucleon mass.

As in Refs. [26,30], the total nuclear response is expressed as

$$S^{ab}(\omega,q) = -\frac{1}{\pi}\int_0^{R_c} dr\frac{{\rm Im}\Pi^{ab}(\omega,q;r)}{\rho(r)}\frac{dP(r)}{dr} \Big/ \int_0^{R_c} dr\frac{dP(r)}{dr}\,, \quad (13)$$

where R_c is the radius at the nuclear surface (defined below), and $dP(r)/dr$ (defined in Refs. [26,30]) represents the probability for the kaon to sample the nucleus per unit radius, accounting for the finite nuclear mean free path of the K^+. The LDA used here is similar to the method described in Refs. [26,30], but there are differences in the parametrizations chosen for $M^*(r)$ and $k_F(r)$ as well as in the definition of R_c. Here the local Fermi momentum is given by

$$k_F(r) = \left(\frac{3\pi^2\rho(r)}{2}\right)^{1/3}, \quad (14)$$

and the local effective nucleon mass is given by [31–33]

$$M^*(r) = M - \left(\frac{2}{\pi^2}\right)\left(\frac{g_s}{m_s}\right)^2 \times\int_0^{k_F(r)} k^2\,dk\,\frac{M^*(r)}{\sqrt{M^*(r)^2+k^2}}\,, \quad (15)$$

with the parameters g_s and m_s taken from Ref. [33]. For this parametrization of the effective nucleon mass, M^* is less than M and the reduced nucleon mass shifts the calculated responses toward higher nuclear excitation energy and also decreases the peak height (i.e., hardens and

quenches the responses). The average turning radius R_c of the bound nucleons is given by the roots of

$$W(R_c) = \langle Q \rangle, \tag{16}$$

where $\langle Q \rangle$ is the average nuclear binding energy for A nucleons bound in the Woods-Saxon potential

$$W(r) = \frac{V_0}{1 + e^{(r - R_0)/a_0}}, \tag{17}$$

and the parameters V_0, R_0, and a_0 have been taken from Ref. [34]. The radial point R_c is the average single nucleon turning point, chosen as the boundary enclosing the region occupied by the bound nucleons. Values of $\langle Q \rangle = -15.4$ MeV and $R_c = 3.1$ fm were found for C, and $\langle Q \rangle = -17.1$ MeV and $R_c = 4.3$ fm were found for Ca.

The correlated RPA polarization insertions have been computed using the σ-ω model [33] of N-N correlations. The N-N potential is assumed to have an attractive piece mediated by the exchange of a neutral isoscalar scalar σ meson and a repulsive part due to the exchange of a neutral isoscalar vector ω meson. One pion exchange is not included since it does not significantly contribute to the ground state properties of nuclear matter [33] from which the σ-ω model is derived. Correlations have been considered in the isoscalar channel ($\Delta T = 0$) only, since the effects of isovector ($\Delta T = 1$) correlations in this momentum transfer range are small, as shown by the pion SCX work of Ref. [26]. For all the RPA calculations, the meson-nucleon couplings and meson masses have been taken from Ref. [33]. Use of the σ-ω model is restricted to isospin symmetric nuclei.

C. Comparison between the calculations and the data

We begin with a comparison to Fermi gas calculations. In this model noninteracting nucleons are assumed to occupy momentum states uniformly up to a maximum momentum k_F. Fermi gas calculations may be expected to work most poorly for light nuclei and better for heavy nuclei like Pb. As with all calculations that ignore N-N calculations, the results should be better for large q, where the effects of N-N correlations are less important.

The relativistic Fermi gas nuclear polarization insertions have been computed in a one-loop approximation utilizing free-particle nucleon wave functions. The individual Fermi gas responses S_0^{ab} are shown in Fig. 11. They have been computed for a momentum transfer of 480 MeV/c using a Fermi momentum of 270 MeV/c, which is appropriate for Pb. All the responses have roughly the same shape and strength, except for the transverse response S^{11}, which is much weaker than the others. Each Fermi gas response function peaks at a nuclear excitation energy of around 120 MeV. For comparison, the dashed line in Fig. 11 shows the nonrelativistic Fermi gas prediction of Ref. [35]. For excitation energies above the region of Pauli blocking, the shape of the nonrelativistic nuclear response function is parabolic.

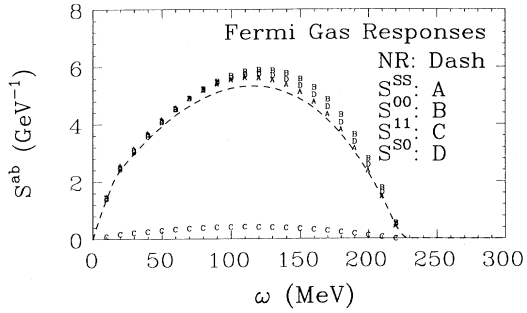

FIG. 11. The individual Fermi gas responses S^{SS}, S^{00}, S^{11}, and S^{S0} are shown with the symbols A, B, C, and D, respectively. The nonrelativistic Fermi gas response of Ref. [32] is shown with a dashed line for comparison. This calculation was done for a fixed three-momentum transfer of 480 MeV/c using the bare nucleon mass of 939 MeV/c^2 and a Fermi momentum of 270 MeV/c. The individual responses each peak at an excitation energy around 120 MeV.

However, the individual relativistic responses S^{ab} are not parabolic due to the vertex operators θ^a [see Eq. (11)] and because relativistic kinematics have been used.

In Fig. 4, the uncorrelated Fermi gas response calculation for Pb at 480 MeV/c is compared to the experimental data. The solid line shows the sum of the isoscalar ($\Delta T = 0$, dashed) and isovector ($\Delta T = 1$, dotted) pieces. The isoscalar and isovector responses have similar shapes, with the isoscalar response contributing about twice as much as the isovector response. While the individual responses shown in Fig. 11 all peak at an excitation energy of about 120 MeV, the summed cross section peaks at a much lower excitation energy of around 100 MeV, because of strong interference between the sum of the first two terms and the third term in Eq. (9). Similar interference effects occur for all the calculations shown in this work. The Fermi gas calculation matches the data to some extent, with poor agreement on the low ω side of the peak and better agreement on the high ω side.

Examples of local density approximation random phase approximation (LDA-RPA) calculations are compared to the C and Ca data in Figs. 2 and 3. At the highest momentum transfer of 480 MeV/c, as shown in the upper panels of Figs. 2 and 3, the agreement with the data is quite satisfactory. Even though discrete excitations cannot be predicted by the LDA used for these calculations, the model does quite well at this momentum transfer since the scattering is nearly incoherent. In the middle panel of Fig. 2 the shape of the quasielastic peak for C is matched by this calculation. At this intermediate momentum transfer of 390 MeV/c slight collective nuclear effects are evident. Calculations at the lowest-momentum transfer of 290 MeV/c are shown for C and Ca in the lower panels of Figs. 2 and 3. At this momentum transfer the quasielastic peak is greatly overshadowed by the collective strength concentrated at much lower ω. For both C and Ca the calculations are in good agreement with the broad, featureless tail of the peak for ω >50 MeV, while again the discrete states cannot be

predicted using this LDA-RPA method. A finite nucleus calculation, as shown in Ref. [13], is required to predict discrete states. However, even in that work, the low-lying excited levels were still underestimated.

V. CONCLUSIONS

Quasielastic scattering of K^+ mesons with an incident laboratory beam momentum of 705 MeV/c from targets of D, C, Ca, and Pb has been studied at fixed three-momentum transfers of 290, 390, and 480 MeV/c. The K^+ quasielastic peak dominates the nuclear excitation energy spectrum near the peak location expected for the kinematic conditions of free K^+-N scattering at 480 MeV/c. However, at 290 MeV/c, mainly due to the strong effects of isoscalar N-N correlations, the quasielastic strength is concentrated at nuclear excitation energies much lower than the peak location expected for free scattering. This coherent effect is not so profound at 390 MeV/c, providing data at a momentum transfer which is between the regimes of strongly collective scattering and incoherent scattering.

The most noteworthy advantage of K^+ quasielastic scattering over other hadronic quasielastic measurements is the long mean free path of positive kaons in nuclear matter, allowing for comparatively deep nuclear penetration. For example, the K^+ reaches a nuclear density in Pb which is 55% of the central density. We found that the experimental effective number of nucleons for K^+ quasielastic scattering greatly exceeds the measured effective number of nucleons for 500 MeV pion reactions on the same targets at the same q. This is not due to medium modifications to the scattering, which we show to compensate nearly completely for our data.

Local density approximation calculations with the random phase approximation including N-N correlations treated in the isoscalar σ-ω model agree with the overall features of the inclusive K^+ spectra for excitation energies above the region of low-lying excited states for C and Ca. Since the K^+ excites nuclear responses which the electron does not, these theoretical interpretations have significantly extended the range of success of σ-ω RPA models. It will be interesting to compare these new data to other calculations based on different models of nuclear dynamics as these may give a closer match to the detailed shape of the measured spectra.

ACKNOWLEDGMENTS

This research was supported in part by the National Science Foundation and in part by the U.S. Department of Energy under Contracts DE-FG02-86ER40269 and DE-AC02-76CH00016. We are sincerely grateful to the scientists and staff at Brookhaven National Laboratory who kept the laboratory and accelerator facilities in working order during this experiment, and we thank W. Jameson and M. Holcomb for their assistance. Comments from A. Gal have been especially illuminating. We further acknowledge the financial support of the U.S.–Japan Cooperative Science Program for the Promotion of Science.

[1] E. J. Moniz *et al.*, Phys. Rev. Lett. **26**, 445 (1971).
[2] B. Frois and C. N. Papanicolas, Annu. Rev. Nucl. Part. Sci. **37**, 133 (1987).
[3] J. E Wise *et al.*, Phys. Rev. C **48**, 1840 (1993).
[4] J. Ouyang, S. Høibråten, and R. J. Peterson, Phys. Rev. C **47**, 2809 (1993).
[5] R. E. Chrien *et al.*, Phys. Rev. C **41**, 1062 (1990).
[6] D. L. Prout, Ph.D. thesis, University of Colorado, Boulder, Colorado, 1992; D. L. Prout *et al.*, to be submitted to Phys. Rev. C (1994).
[7] J. Bergqvist *et al.*, Nucl. Phys. **A469**, 648 (1987).
[8] R. E. Chrien *et al.*, Phys. Rev. C **21**, 1014 (1980).
[9] Ya. A. Berdnikov, A. M. Makhov, and V. I. Ostroumov, Yad. Fiz. **52**, 3 (1990) [Sov. J. Nucl. Phys. **52**, 1 (1990)].
[10] Ya. A. Berdnikov, A. M. Makhov, V. I. Ostroumov, and A. P. Shishlo, Yad. Fiz. **53**, 3 (1991) [Sov. J. Nucl. Phys. **53**, 1 (1991)].
[11] R. A. Arndt and L. D. Roper, "Scattering Analysis Interactive Dial-in," Report No. CAPS–80–3 (unpublished), Center for Analysis of Particle Scattering, Virginia Polytechnic Institute and State University, Blacksburg, VA (1983); R. A. Arndt, Z. Li, L. D. Roper, R. L. Workman, and J. M. Ford, Phys. Rev. D **43**, 2131 (1991).
[12] W. O. Lock and D. F. Measday, *Intermediate Energy Nuclear Physics* (Methuen, London, 1970).
[13] C. M. Kormanyos *et al.*, Phys. Rev. Lett. **71**, 2571 (1993).
[14] C. M. Kormanyos, Ph.D. thesis, University of Colorado, 1994.
[15] R. J. Glauber and G. Matthiae, Nucl. Phys. **B21**, 135 (1970).
[16] G. F. Bertsch and O. Scholten, Phys. Rev. C **25**, 804 (1982).
[17] H. de Vries, C. W. de Jager, and C. de Vries, At. Data Nucl. Data Tables **36**, 495 (1987).
[18] C. Wilkin, in *Proceedings of the Banff Summer School on Intermediate Energy Nuclear Physics*, edited by G. C. Neilson, W. C. Olsen, and S. Varma (Nuclear Research Centre, Department of Physics, Alberta, 1970).
[19] D. Marlow *et al.*, Phys. Rev. C **25**, 2619 (1982).
[20] R. Sawafta *et al.*, Phys. Lett. B **307**, 293 (1993); R. Weiss *et al.*, Phys. Rev. C **49**, 2569 (1994).
[21] P. B. Siegel, W. B. Kaufman, and W. R. Gibbs, Phys. Rev. C **30**, 1256 (1984).
[22] G. E. Brown, C. B. Dover, P. B. Siegel, and W. Weise, Phys. Rev. Lett. **60**, 2723 (1988).
[23] Y. Mardor *et al.*, Phys. Rev. Lett. **65**, 2110 (1990).
[24] J. Labarsouque, Nucl. Phys. **A506**, 539 (1990).
[25] J. C. Caillon and J. Labarsouque, Phys. Rev. C **45**, 2503 (1992).
[26] J. Ouyang, S. Høibråten, and R. J. Peterson, Phys. Rev.

C **48**, 1074 (1992).
[27] J. Ouyang, Ph.D. thesis, University of Colorado, 1992, Los Alamos Report No. LA-12457-T (unpublished).
[28] R. J. Peterson *et al.,* Phys. Lett. B **297**, 238 (1992).
[29] H. Tyrén, P. Hillman, and T. A. J. Maris, Nucl. Phys. **7**, 10 (1958); H. Tyrén, S. Kullander, D. Sundberg, R. Ramachandran, P. Isacsson, and T. Berggen, Nucl. Phys. **79**, 321 (1966).
[30] U. Stroth *et al.*, Phys. Lett. **156B**, 291 (1985).
[31] H. Kurasawa and T. Suzuki, Nucl. Phys. **A445**, 685 (1985).
[32] C. J. Horowitz and J. Piekarewicz, Nucl. Phys. **A511**, 461 (1990).
[33] B. D. Serot and J. D. Walecka, Adv. Nucl. Phys. **16**, 1 (1986).
[34] W. M. Alberico, P. Czerski, M. Ericson, and A. Molinari, Nucl. Phys. **A462**, 269 (1987).
[35] A. L. Fetter and J. D. Walecka, *Quantum Theory of Many-Particle Systems* (McGraw-Hill, New York, 1971).